Increased radon exposure from thawing of permafrost due to climate change

Paul W.J. Glover
School of Earth and Environment, University of Leeds, Leeds, LS2 9JT, UK

Key Points

1. Modeling shows that permafrost acts as a radon barrier, reducing radiation to a tenth of the background level, and increasing it behind the barrier.
2. Instantaneous permafrost thawing gives plumes >200 Bq/m^3 lasting over 5 years in buildings with basements, but no increase in pile-supported buildings.
3. Radiation plumes over 200 Bq/m^3 for up to 4 years also occur when slower thawing that results in 40% melt in less than 15 years is modeled.

Abstract

Radon is a natural radioactive gas accounting for approximately one in ten lung cancer deaths, with substantially higher death rates in sub-Arctic communities where smoking is more prevalent. Radon transport is significantly reduced in permafrost, but permafrost is now thawing due to climate change. The effect of permafrost thawing on domestic radon exposure is unknown. Here we present results from radon transport modelling through soil, permafrost and model buildings either with basements or built on piles. We find that permafrost acts as an effective radon barrier, reducing radiation exposure to a tenth of the background level, while producing a ten-fold increase in the radon activity behind the barrier. When we model thawing of the permafrost barrier, we find no increase in radon to the background level for buildings on piles. However, for buildings with basements the radon increases to over one hundred times its initial value and can remain above the 200 Bq/m^3 threshold for up to seven years depending on the depth of the permafrost and the speed of thawing. When thawing speed is taken into account, radiations remains higher than the threshold for all scenarios where 40% melting occurs within 15 years. This new information suggests that a significant sub-Arctic population could be exposed to radon levels dangerous to health as a result of climate change thawing of permafrost, with implications for health provision, building codes and ventilation advice.

Plain Language Summary

Radon is an invisible natural radioactive gas which causes approximately one in ten lung cancer deaths. It affects smokers much more than non-smokers and causes higher death rates in sub-Arctic communities where smoking is more common. Radon flow is significantly reduced by permafrost, but permafrost is now thawing due to climate change. This paper models flow of radon through soil, permafrost and model buildings either with basements or on piles. We find that permafrost acts as an effective radon barrier. It reduces radiation to about a tenth of the background level. The trapped radon produces increases radiation behind the barrier. When we model thawing of the permafrost barrier, we find no increase in radon to the background level for buildings built on piles. However, for buildings with basements the radon increases to more than one hundred times its initial value for up to seven years depending on the depth of the permafrost and how fast the permafrost melts. This new information suggests that a significant sub-Arctic population could be exposed to radon levels dangerous to health as a result of permafrost thawing due to climate change. This has implications for health provision, building codes and ventilation advice.

1. Introduction

The National Council on Radiation Protection and Measurements has identified naturally occurring radon as the largest source of environmental radiation to persons living in the United States and the second leading cause of lung cancer after smoking (Nitzbon et al., 2020; Dela Cruz et al., 2011). It has been estimated to cause between 8,000 and 45,000 lung cancer deaths per year (Pawel and Puskin, 2003; Al-Zoughool and Krewski, 2009). Radon causes approximately 10-14% of lung cancer deaths in USA (WHO, 2019; Lubin et al., 2004; Krewski et al., 2006; Krewski et al., 2005; BEIR VI, 1999) and about 3.3-8.3% in Europe (WHO, 2009; Darby et al., 2005; Darby et al., 2006).

Radon is produced from rocks and soils containing significant concentrations of U^{238} and its decay products (Peto and Darby, 1994). It is transported through the rocks and soils by diffusion and advection (Chen et al., 1995; Othman et al., 2021), ultimately being either dispersed harmlessly in the atmosphere or leaching into buildings through their foundations where high concentrations can accumulate if the building is not ventilated (Chung et al., 2020). The worldwide average (UNSCEAR, 2000) Ra^{226} activity is 39 Bq/kg. The diffusive and advective transport of radon through the soil is

62 controlled by the porosity, fluid saturations, diffusion coefficients and relative permeabilities of the
63 soil. All of these parameters are expected to be reduced significantly in permafrost (Fortin et al., 2007).
64 Since permafrost makes up about one fifth of the Earth's terrestrial surface (Worsley, 1986), it
65 would be expected that buildings constructed on permafrost might be protected to some degree by the
66 permafrost acting as a radon barrier. It might also be expected that rapid permafrost melting (Nitzbon
67 et al., 2020), that is now occurring as a result of climate change (Witze, 2020; Yumashev et al., 2019),
68 might expose people living or working in buildings that were once underlain by permafrost to increase
69 concentrations of radon as well as leading to further releases of carbon (Turetsky et al., 2020).
70 The global cryosphere, defined as all of the areas on Earth with frozen water, shrank on average by
71 about 87,000 km^2 per year (about 33,000 square miles per year), between 1979 and 2016 as a result of
72 climate change according to a recent study (Peng et al., 2021). It has also been recently estimated that
73 5 million people live on permafrost in the Arctic Circumpolar Permafrost Region (ACPR), of which
74 42% will become permafrost-free due to climate-driven thawing by 2050, affecting 3.3 million
75 inhabitants (Ramage et al., 2021). The solid geology of these northern polar regions is predominantly
76 composed of metamorphic and plutonic terranes (Petrov and Pubellier, 2018) that contain raised levels
77 of U^{238} and its decay products (Scheib et al., 2009), exacerbating the risk.
78 Sociological factors need also to be taken into account. It is well recognised that radon-acquired
79 lung cancer is about 26 times (25.8+5.4/-4.5) more prevalent in tobacco smokers than it is for non-
80 smokers (Darby et al., 2005; Lubin et al., 2004; Krewski et al., 2006). This is especially important
81 considering that the prevalence of smoking in the Arctic has always been high (79% for the Inuit of
82 Greenland in 1997 (Bjerregaard et al., 1997), 62.3% for the Inuit of Canadian Arctic in 2012). Sparsity
83 of data means that more recent estimates are not available, but though likely to be smaller, still
84 considerably higher than recent values of 17.8%, 23% and 16.3% for the UK, EU and USA,
85 respectively (WHO, 2009). It seems that, in arctic Canada at least, the population is likely to be more
86 sensitive to increases in domestic and work-place radon as a result of their lifestyle. This may be
87 balanced to some extent by the style of buildings that predominate. In northern areas it is more

common for buildings to be raised off the ground on piles, with natural ventilation occurring below the building (Buijze and Wright, 2021). This type of construction would be naturally immune to radon.

Little is known about the transport of radon in soils and especially in permafrost. In this modelling we use the best values we can obtain in order to numerically model the transport of radon from the soil and into several types of building in the presence of a permafrost layer and when the permafrost has melted.

2 Methods

2.1 Model

All modelling is carried out by the finite element solution of linked partial differential equations in two dimensions and as a function of time using Comsol Multiphysics®. An example of the physical models used is shown in Figure 1. Each is 60 m wide and includes a 45 m depth of soil. The permafrost layer for each calculation has uniform thickness, which has been varied between 0.5 m and 5 m in 0.5 m steps. The unfrozen topsoil layer has been assumed to be of uniform thickness, and has been varied between 0 m and 15 m thick in four steps. There are four soil domains; (a) soil below the permafrost layer, (b) the permafrost layer, (c) the soil above the permafrost layer on each side of the building.

The model buildings are each split into three domains. For the modern building style, the domains are; (i) a rectangular basement (3 m high, 18 m wide), which is just below the surface of the soil and penetrates into the permafrost layer, (ii) a rectangular main living space (10 m high, 18 m wide), and (iii) a triangular roof space (5 m high, 18 wide). For the traditional style of building, the domains are; (i) a ventilated underfloor space (2 m high, 18 m wide), which contains piles that penetrate into the permafrost layer, (ii) a rectangular main living space (10 m high, 18 m wide), and (iii) a triangular roof space (5 m high, 18 wide).

A two dimensional mesh is created and refined in all domains of the model. The mesh consists of triangles which have side lengths no larger than 1 m in the body of the model, and no larger than 0.2 m along all boundaries except those where the boundary conditions of insulation and symmetry are

applied, where they are no larger than 0.5 m. There are about 25,000 elements in the final model. The number of elements controls the speed of the final solution. We found that the solutions were reached within several minutes on a standard 3 GHz laboratory PC, and hence retain the described geometry for clarity even though the model is symmetric and could be reduced to half of its size.

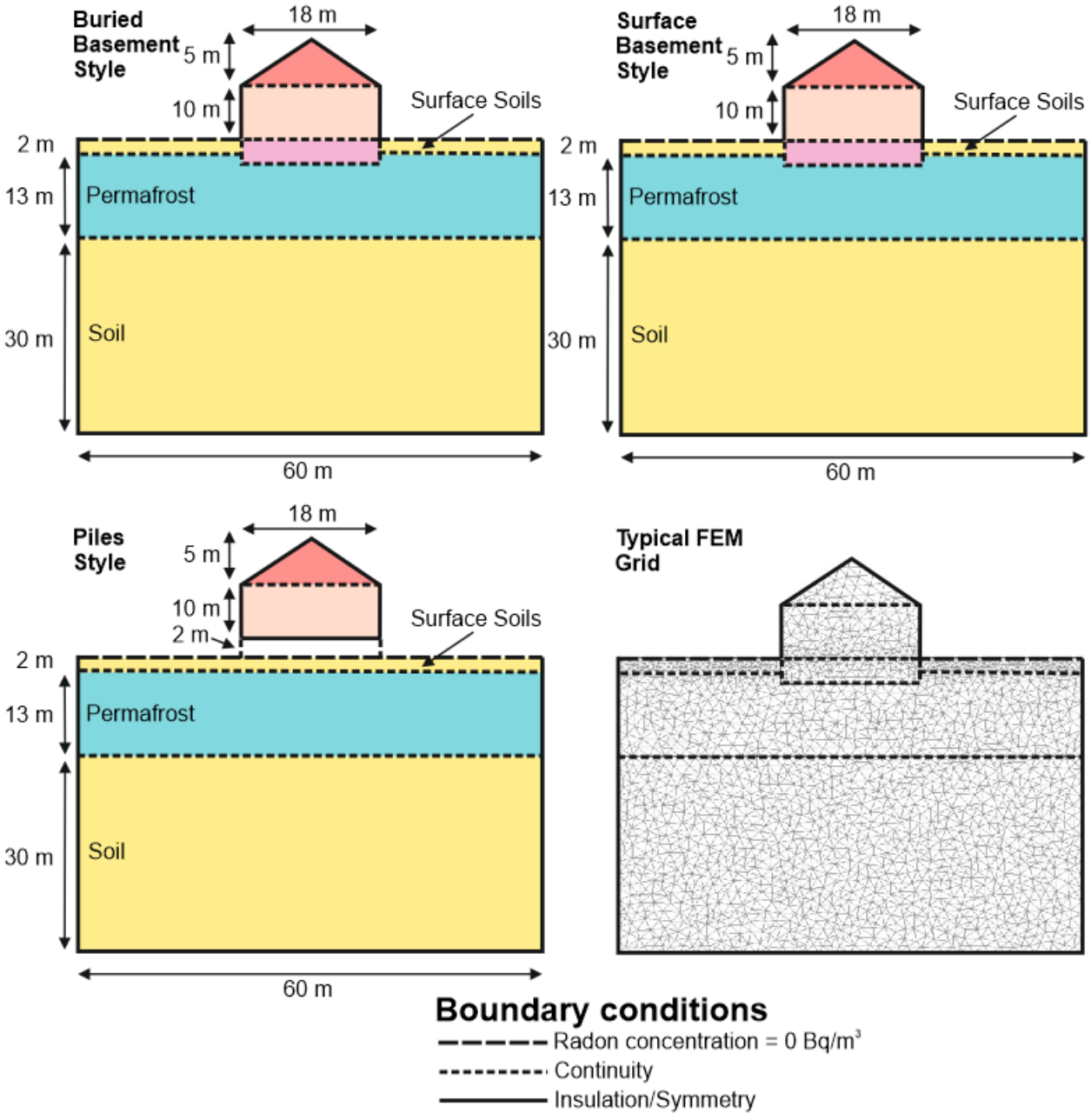

Figure 1. The geometries of the two models tested in this work with dimensions, boundary conditions and an example FEM mesh.

2.2 Differential Equations

The fundamental differential equations follow from Fick's and Darcy's laws, and Laplace's equation:

$$\vec{J}_{diff,a} = -(1 - S_w)\phi\tau_a D_a \nabla C_a \quad \textbf{[1]}$$

$$\vec{J}_{diff,w} = -S_w\phi\tau_w D_w \nabla C_w \quad \textbf{[2]}$$

$$\vec{J}_{adv,a} = -C_a \frac{k_a}{\mu_a} \nabla P \quad \textbf{[3]}$$

$$\nabla^2 P = 0 \quad \textbf{[4]}$$

where J are the bulk fluxes of radon (Bq m^{-2} s^{-1}), the subscripts *adv* and *diff* refer to advection and diffusion respectively, and a, w, i and s refer to air, water, ice and solid surfaces, S_w is the water saturation of the pore space (fractional), ϕ is the porosity of the soil (fractional), τ are the tortuosities of the radon flow (fractional) in each phase, D_w and D_a are the diffusion coefficients of radon in water and air (m^2 s^{-1}), k_a is the intrinsic permeability to air (m^2), μ_a is the dynamic viscosity of air, C_w and C_a are the radon concentrations in each phase (Bq m^{-3}), and P is the gas pressure (Pa).

It is assumed that radon is generated within the soil and permafrost at a rate $\Sigma[\text{Bq m}^{-3}\text{ s}^{-1}] = \eta\rho_b\lambda C^{Ra226}$, which is constant in space (i.e., the same in all soils and permafrost and zero elsewhere) and in time (Gadd and Borak, 1995), where η is the sum of the fractional emanation coefficients into the air, water, ice and adsorbed phase ($\eta = \eta_{air} + \eta_{water} + \eta_{ice} + \eta_{surface}$), ρ_b is the soil bulk density (kg m^{-3}), λ is the decay constant of radon (s^{-1}) and C^{Ra226} is the radium-226 activity per unit dry mass (Bq kg^{-1}).

The mass balance equations for each phase (air, water, ice and solid surfaces, respectively) are:

$$(1 - S_w - S_i)\phi \frac{\partial C_a}{\partial t} = \nabla \cdot \left((1 - S_w - S_i)\phi\tau_a D_a \nabla C_a\right) + \frac{k_a}{\mu_a}\nabla P \cdot \nabla C_a - (1 - S_w - S_i)\phi\lambda C_a + \eta_a\rho_b\lambda C^{Ra226} - \sum_{j\neq a}\left(T_{aj} - T_{ja}\right) \quad \textbf{[5]}$$

$$S_w\phi \frac{\partial C_w}{\partial t} = \nabla \cdot (S_w\phi\tau_w D_w \nabla C_w) - S_w\phi\lambda C_w + \eta_w\rho_b\lambda C^{Ra226} - \sum_{j\neq w}\left(T_{wj} - T_{jw}\right) \quad \textbf{[6]}$$

$$S_i\phi \frac{\partial C_i}{\partial t} = \nabla \cdot (S_i\phi\tau_i D_i \nabla C_i) - S_i\phi\lambda C_i + \eta_i\rho_b\lambda C^{Ra226} - \sum_{j\neq i}\left(T_{ij} - T_{ji}\right) \quad \textbf{[7]}$$

$$\rho_b \frac{\partial C_s}{\partial t} = -\rho_b\lambda C_s + \eta_s\rho_b\lambda C^{Ra226} - \sum_{j\neq s}\left(T_{sj} - T_{js}\right) \quad \textbf{[8]}$$

Advection is assumed negligible for the water and ice phases, while both diffusion and advection are assumed to be negligible for the solid phase at the timescales covered by this modelling. Note that the units of C_s are exceptionally Bq kg^{-1}.

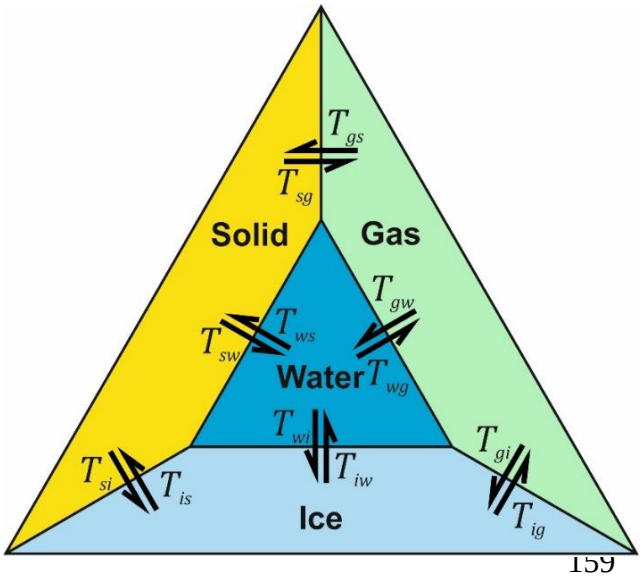

Figure 2. Transfer coefficients $T_{jk} = \alpha_{jk}\Gamma_j C_j$ and their relationship with the 4 phases present in permafrost.

The radon will distribute itself between all four phases by sorption and solution. This process is described by transfer coefficients T_{jk} (Bq m^{-3} s^{-1}), which are defined as the rate of transfer of radon activity per unit volume from phase j to phase k. The first order transfer coefficients are given by $T_{jk} = \alpha_{jk}\Gamma_j C_j$, where $j, k \in \{a,w,i,s\}$, α_{jk} are exchange rates (s^{-1}), C_j are radon concentrations, and Γ_j is a multiplier ($\Gamma_j = (1 - S_w - S_i)\phi$, $S_w\phi$, $S_i\phi$, and ρ_b for j=$\{a,w,i,s\}$, respectively. The transfer coefficient are shown schematically in Figure 2.

By assuming that (i) adsorption to wet surfaces or ice is negligible, (ii) exchange between water, air and ice phases occurs at a timescale much shorter than those typical of radon transport, and (iii) exchange between the air and solid surface adsorbed phase is fast or negligible, it is possible to follow a reduction similar to that by Rogers and Nielson (1991a; 1991b). Water has a much larger affinity to most minerals than radon, so assumption (i) is reasonable. Typical exchange times between air and water are estimated to be between 0.1 and 10 seconds for water layers 10 to 100 μm thick, which is considerably shorter than the timescales involved with concentration changes due to diffusion and advection in soils (hours to days), substantiating the second assumption for water and air. As for the degree of adsorption or absorption of radon molecules on ice surfaces, a comparison of the

experimentally determined adsorption enthalpy of radon on ice of -19.2±1.6 kJ/mol (Eichler et al., 2000) with the adsorption enthalpies of radon on other solid state surfaces, the solution enthalpy of radon in water, and the formation enthalpy of a hypothetical radon clathrate hydrate shows that with a high probability radon is adsorbed as a free atom on the ice surface and is not fully coordinated by water dipoles. We can find no data to support assumption (ii) for exchange between ice and air or water.

Consequently, the linked partial differential equations reduce to:

$$\gamma \frac{\partial C_a}{\partial t} = \nabla \cdot (D \nabla C_a) + \frac{k_a}{\mu_a} \nabla P \cdot \nabla C_a - \gamma \lambda C_a + \Sigma \quad \textbf{[9]}$$

where: $\gamma = (1 - S_w - S_i + S_w L_{aw} + S_i L_{ai})\phi + \rho_b k_a$ is the operating porosity,

$D = \left((1 - S_w - S_i)\tau_a D_a + S_w \tau_w D_w L_{aw} + S_i \tau_i D_i L_{ai}\right)\phi$ is the effective diffusion coefficient,

and $\Sigma = \eta \rho_b \lambda C^{Ra226}$ is the source term.

The parameters L_{aw} and L_{ai} are Ostwald coefficients, τ_j are tortuosities, D_j are diffusion coefficients and S_j are phase fractions for each phase. In this work we set C^{Ra226}=40 Bq/kg, which is a conservative 33% of the range 10-100 Bq/kg given by Nazaroff (1992) in his review for mean soils in the USA, and η=0.2, which is cited as typical for soils after compiling emanation coefficients for soils from 13 sources (Nazaroff, 1992). For simplicity the thawing assumes all ice thaws to water with no change in porosity, which implies that in this model there is no compaction of soil upon thawing nor radon pumping from the compaction process. We were unable to find diffusion coefficient data for radon in ice. However, observations of diffusion of CO_2 through ice in the field vary between 2.45×10^{-10} m^2/s and 1.41×10^{-10} m^2/s, increasing with temperature (Ahn et al., 2008) and between 1.1×10^{-11} m^2/s and 3×10^{-11} m^2/s at 270 K for diffusion parallel and perpendicular to the *c*-axis, respectively (Ikeda-Fukazawa et al., 2004a; 2004b). Consequently we have assumed that the mean diffusion coefficient of radon in ice at 270K can be represented by a value of 2×10^{-11} m^2/s. Since this value is about 100 times less than the diffusion coefficient for radon in water, even a large error will be insignificant in the modelling.

2.3 Boundary Conditions and Assumptions

The boundary conditions are shown in Figure 1. All lateral soil boundaries were set to insulation/symmetry conditions as was the lower boundary of the model. The outer walls of the building were set to insulation/symmetry for an unventilated building and to C_a=0 Bq/m^3 for a fully ventilated building. Boundaries within the building and between the soil and permafrost were set to represent continuity in the radon concentration, and the soil surface boundary condition was C_a=0 Bq/m^3. Boundaries between the soil or permafrost and the basement of the building were initially set to represent continuity in the radon concentration. This last assumption was made for simplicity. All models include 0.3 m thick basement walls whose boundaries represent radon concentration continuity, but whose porosity, diffusion coefficient and gas permeability are taken from those of concrete (Cozmuta et al., 2003).

Table 1. Modelling parameters

	Value Before Melt	Value After Melt	Units	Source/Notes
S_w	0	0.9	-	Imposed
S_i	0.9	0	-	Imposed
L_{aw}	0.253	0.253	-	Ongori et al. (2015)
L_{ai}	0.253	0.253	-	Assumed = L_{aw}
ϕ	0.245	0.245	-	No compaction
ρ_b	2.22×10^{3}	2.25×10^{3}	kg/m^3	Calculated with ρ_{ma}=2650 kg/m^3
k_a	9.87×10^{-17}	9.87×10^{-20}	m^2	Chuvilin et al. (2021)
τ_a	7	7	-	Moldrup et al. (2000)
τ_i	1	7	-	Moldrup et al. (2000)
τ_w	7	1	-	Moldrup et al. (2000)
D_{air}	1.1×10^{-5}	1.1×10^{-5}	m^2 s^{-1}	Barrio-Parra et al. (2022)
D_i	2.0×10^{-11}	2.0×10^{-11}	m^2 s^{-1}	Ahn et al. (2008); Ikeda-Fukazawa (2004a; 2004b)
D_w	1.3×10^{-9}	1.3×10^{-9}	m^2 s^{-1}	Barrio-Parra et al. (2022)
η	0.2	0.2	-	Cozmuta et al. (2003)
λ	2.1×10^{-6}	2.1×10^{-6}	s^{-1}	Nazaroff (1992)
C^{Ra226}	40	40	Bq kg^{-1}	Cozmuta et al. (2003)

2.4 Scenarios

The scenarios modelled in the study are represented by Table 1. A major challenge has been to obtain values for porosity, diffusion coefficient and gas permeability that are representative of reality. There has been very few experimental determinations of these parameters. A mean value of 0.2 has been assumed for the soil porosities. The Ostwald coefficient for the solution of radon in water is 0.253 at 293 K (Ongori et al., 2015), and that for the solution of radon in ice has been assumed to be the same.

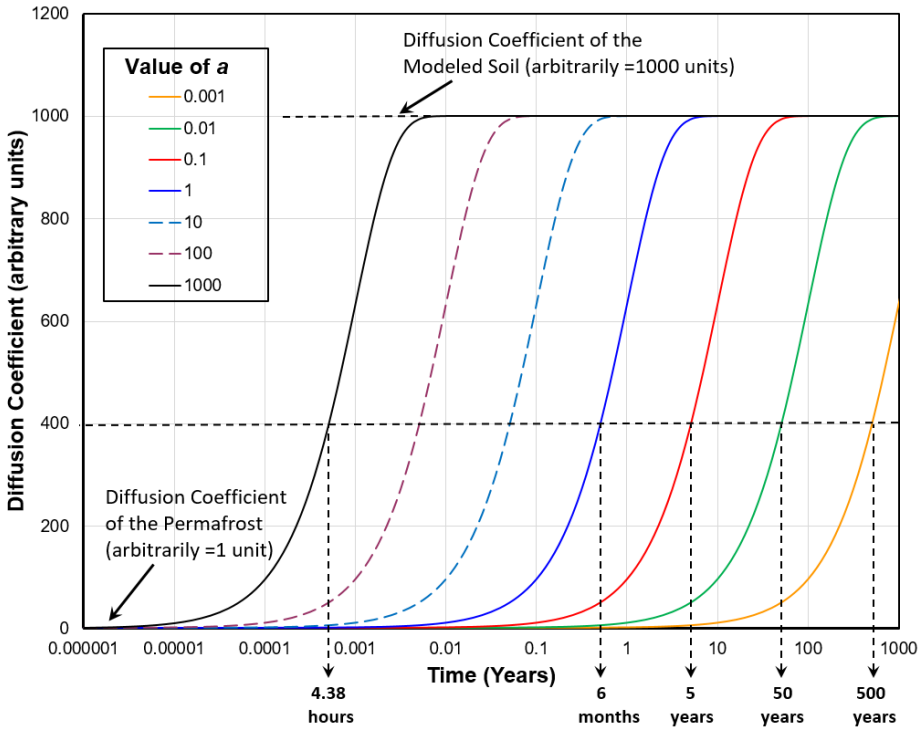

Figure 3. Modelled variation of the effective diffusion coefficient D_{eff} in arbitrary units as a function of time t in years from the diffusion coefficient of fully frozen permafrost (D_p =1 unit) to that of fully defrosted soil (D_s =1000 units) according to $D_{eff} = D_s - (D_s - D_p)e^{-at}$, where a controls the rate of change.

2.5 Modelling Permafrost Melt

We model the changes to the diffusion coefficient of radon through melting permafrost by assuming that the effective diffusion coefficient D_{eff} follows an exponential transition from the diffusion coefficient of the fully frozen permafrost D_p to that of the fully defrosted soil D_s according to $D_{eff} = D_s - (D_s - D_p)e^{-at}$. Here t is the time in years and the exponential coefficient a controls the rate of change. For clarity, we show this behaviour in Figure 3, where arbitrary units have been used for

clarity, with D_p = 1 unit and D_s=1000 units. The solid curves show the scenarios used in this modelling, from quasi-instantaneous melting represented by the black line (40% change after 4.38 hours) to the longest transition represented by the orange line (40% change after 500 years). The curve colours are the same as used for the results in the main body of the paper. The dashed lines show scenarios which were not modelled in this paper.

3. Results

3.1 Permafrost as a Radon Barrier

Here we present results from numerical modelling of radon transport through soil, permafrost and various types of ventilated and unventilated model buildings. Modelling has been carried out for two types of building, for scenarios involving advective and/or diffusive transport, and for different rates of permafrost melting.

Figure 1 shows the two model scenarios that were studied in this work together with boundary conditions and a typical finite element modelling mesh.

Initial modelling was carried out with a 13 m thickness of permafrost in place and the modelling parameters shown in Table 1. We find that the presence of the permafrost acts as an effective radon barrier even in the absence of advective transport. This is the case irrespective of how deep the permafrost barrier is placed, as shown in Figure 4 for the basement style building.

For the world average Ra^{226} activity of 39 Bq/kg (UNSCEAR, 2000), the permafrost reduces the domestic radon concentrations by 80 to 90% (4 to 8 Bq/m^3) while leading to an increase in the concentration in the radon behind the barrier by up to 11.43 times (445.8 Bq/m^3). Consequently, permafrost can provide an effective protection from radon.

This modelling observation accords well with the observations of Conen and Robertson (2002), who report a strong decrease in radon flux from a constant rate of about 1 atom cm^{-2} s^{-1} for all latitudes south of 30°N, decreasing northwards to 0.2 atom cm^{-2} s^{-1} at 70°N.

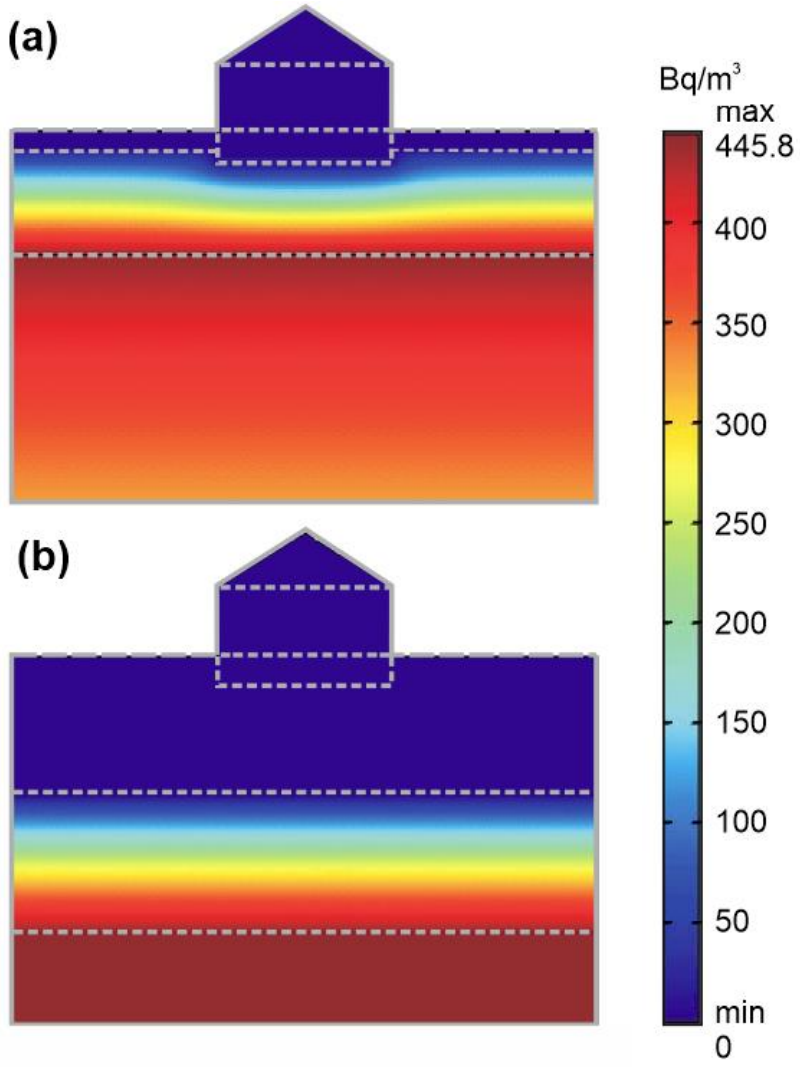

Figure 4. Radon activity distribution is controlled by the 13 m thick permafrost barrier, wherever it is positioned, here (a) 2 m from the surface, or (b) 15 m.

3.2 The Effect of Building Type

Thawing of the permafrost is beginning to occur as a result of global climate change (WHO, 2019; Witze, 2020; Yumashev et al., 2019). When we model this thaw we observe transient plumes of radon passing through some types of building. The plume of radon has an intensity and duration which depends on the style of building, the depth to the permafrost layer, whether advection as well as diffusion plays a part in the radon transport process, and the time taken to melt the permafrost sufficiently for it to become patent to radon.

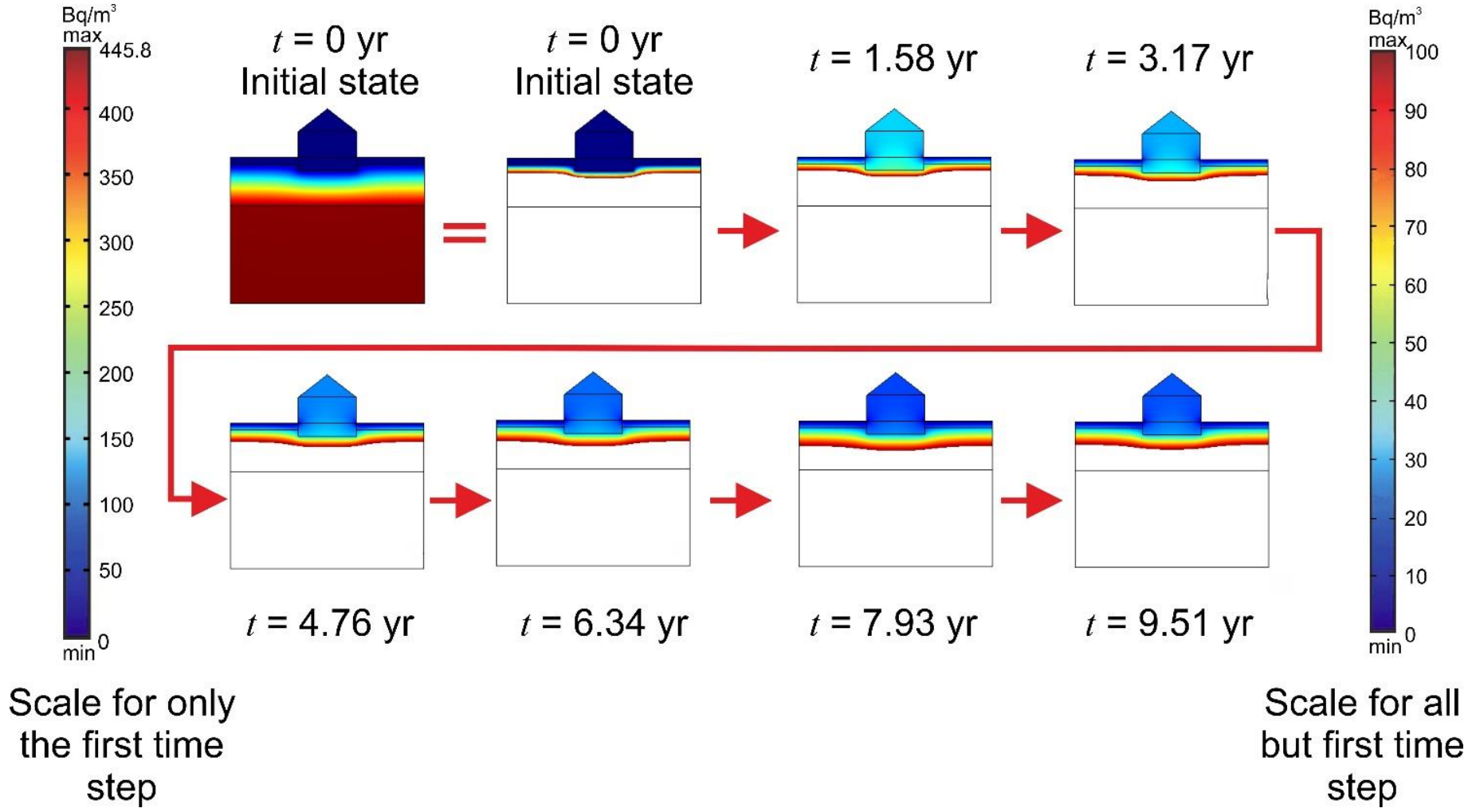

Figure 5. Selected time steps (from 180) showing the radon concentration plume passing through the buried basement-style model building after the quasi-instantaneous melting of the permafrost (left scale for the top-right model, restricted right scale for all of the remaining time steps).

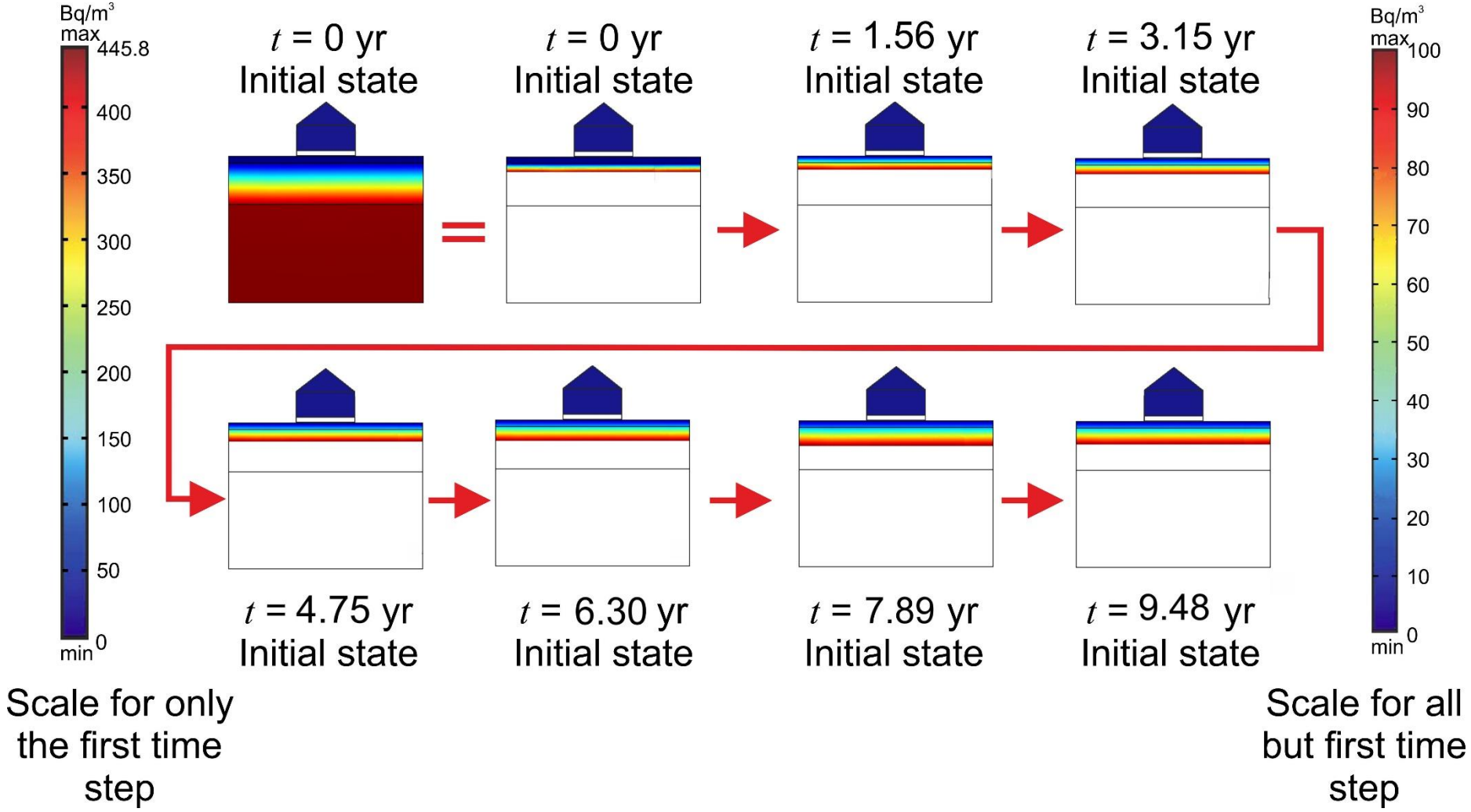

Figure 6. Selected time steps (from 180) showing the radon concentration plume passing through the piles-style model building after the quasi-instantaneous melting of the permafrost (left scale for the top-right model, restricted right scale for all of the remaining time steps).

For the type of building that contains a basement that is buried in the soil, we observe a well-developed plume of radon which lasts over a decade, and is greater than the threshold value of 200 Bq/m^3 for up to about 7 years. Figure 5 shows the temporal variation of this observation as radiation maps for the building and the soil at 8 selected time-steps out of about 180 that resulted from the modelling. A video of the progression of the plume for all rendered time-steps is available by request from the author or from the additional data pages. In this case, the depth to the top of the permafrost is 2 m and the melting of the permafrost is considered to be quasi-instantaneous. The time step parts are shown on a restricted scale to show the radon plume more effectively. In these models the initial values of radon concentration within the building (5 to 10 Bq/m^3) are increased transiently, up to 70-fold, to values of the order of about 350 Bq/m^3 by the passage of the released radon through the building. After a number of years the radon disperses and the value in the building falls to the value that would have been typical if the permafrost layer had not originally occurred (around 39 Bq/m^3 in this modelling) over a period greater than 50 years.

For building having a basement that rests directly on the ground, we observed a temporal variation of the plume that is almost identical to that shown in Figure 5, and hence we do not include it as a separate figure.For buildings raised on piles there was no increase in radon in the building for any of the scenarios. Figure 6 shows the analogue temporal variation in this case. This expected result confirms that buildings built on piles are sufficiently well-ventilated that they do not suffer from radon build-up.

It is recognised that the common practice is for the spaces under pile-supported dwellings to be partially enclosed in order that the space can be used a secure store and to alleviate the ingress of snow. We have not attempted to model this scenario, but we believe that it is unlikely for radon to build-up in these semi-ventilated spaces sufficiently for the insulated building above to see an increase in radon concentration.

3.3 The Effect of Permafrost Depth

The remainder of this paper address buildings with basements that either lie partly or immediately above or within the permafrost.

In the first of these scenarios, we modelled the mean intensity and transience of radon plumes within the building as a function of the depth of the buried permafrost layer for the case where all radon was transported by diffusion, which is the common case, and for a sudden increase of the ability of the permafrost to transport radon. Such an occurrence might be likened to instantaneous melting, but in reality is more likely to occur when sufficient melt has occurred for a radon transport pathway to form.

The resulting data are given in the form of arithmetic mean radon concentration (in Bq/m^3) within the building as a function of time so that the temporal progression of risk due to radon can be tracked more quantitatively and with a better temporal resolution.

Figure 7 shows that both the radon concentration and the period of raised radon concentrations within the building increase as the depth to the permafrost layer decreases. Radon concentrations do not exceed 200 Bq/m^3 for permafrost layers starting at a depth greater than about 9 m. However, for] rost starting at less than this depth, the plume of radon can exceed 350 Bq/m^3 and remain over the 200 Bq/m^3 level for over 6.66 years. The greater depths provide diffusive routes for the radon to disperse and be released to the atmosphere without encountering the building.

3.4 The Effect of Speed of Permafrost Melt

The results in Figure 7 assume an instantaneous transition of the diffusion coefficient for radon from that for permafrost to that for the associated soil. Clearly, this assumption is unrealistic. Consequently we have tested 5 scenarios where the change in the effective diffusion coefficient D_{eff} varies as a function of time as described in the methodology. In these scenarios a 40% increase in diffusion coefficient occurs after 0.5, 5, 50 and 500 years as controlled by an exponential coefficient a=1, 0.1, 0.01 and 0.001, respectively. The results of modelling are shown in Figure 8.

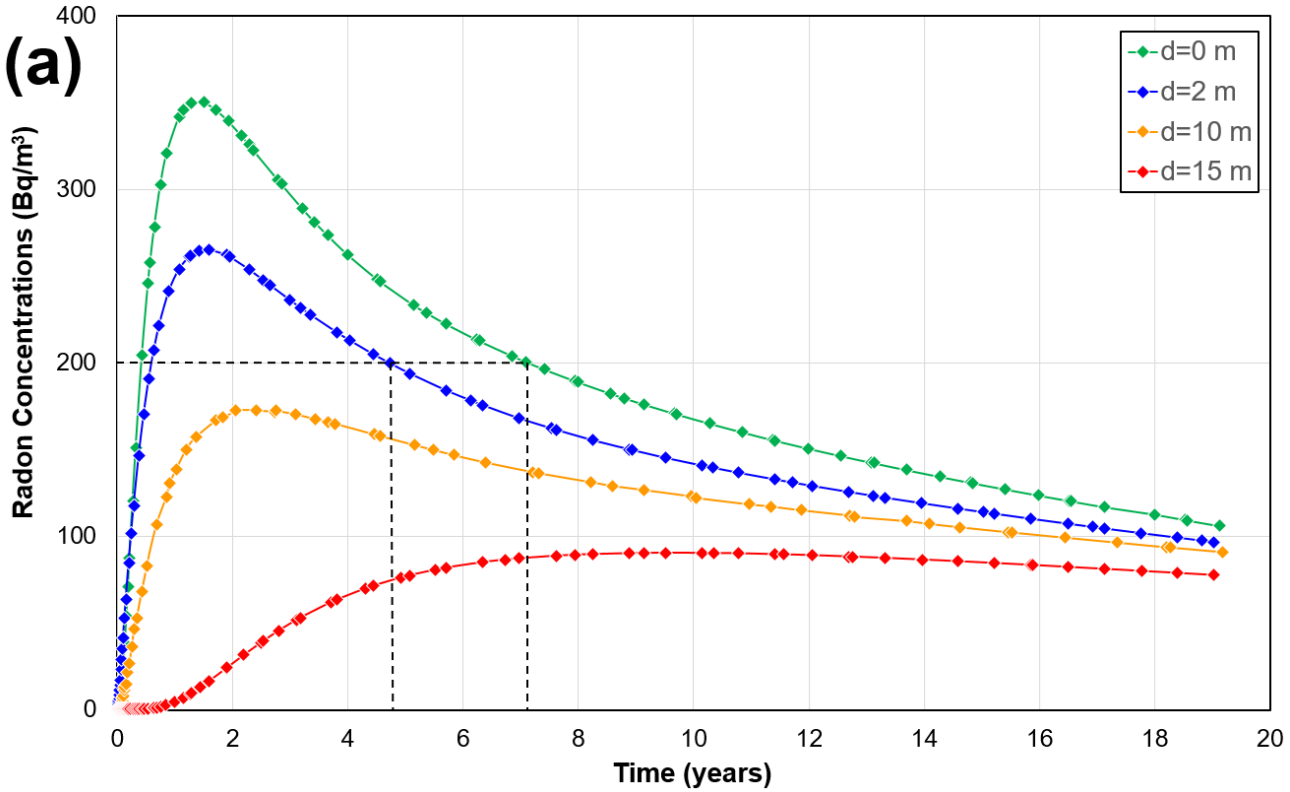

Figure 7. Evolution of arithmetic mean radon concentration within basement style buildings after sudden increase in the ability of permafrost to transport radon by diffusion for four different depths to the top of the permafrost (d=0 m to 15 m).

In all cases radon concentration peak diminishes and spreads out in time as the melt process lengthens. It is expected that this occurs because the longer the timescale, the greater chance that the radon can diffuse laterally 'missing' the building, while the radon already in the building has a greater time to disperse naturally.

The 200 Bq/m^3 threshold is exceeded for all scenarios where a<0.035 which represents a change in effective diffusion coefficient D_{eff} of 40% in 15 years or shorter. In Figure 8 we show the time for which the mean radon concentration in the building is above 200 Bq/m^3 as coloured bars. The period for which the radon concentration is greater than 200 Bq/m^3 is 4.2 years for the quasi-instantaneous case (black, 40% change in the effective diffusion coefficient D_{eff} in 4.38 hours), compared to 4.65 years (blue) for a 40% change in D_{eff} in 6 months, and 4.6 years (red) for a 40% change in D_{eff} in 5 years. The longer it takes to reach 40% change in effective diffusion coefficient, the lower the peak

radon concentration, until about 15 years, whereupon the peak radon concentration never exceeds the 200 Bq/m^3 threshold

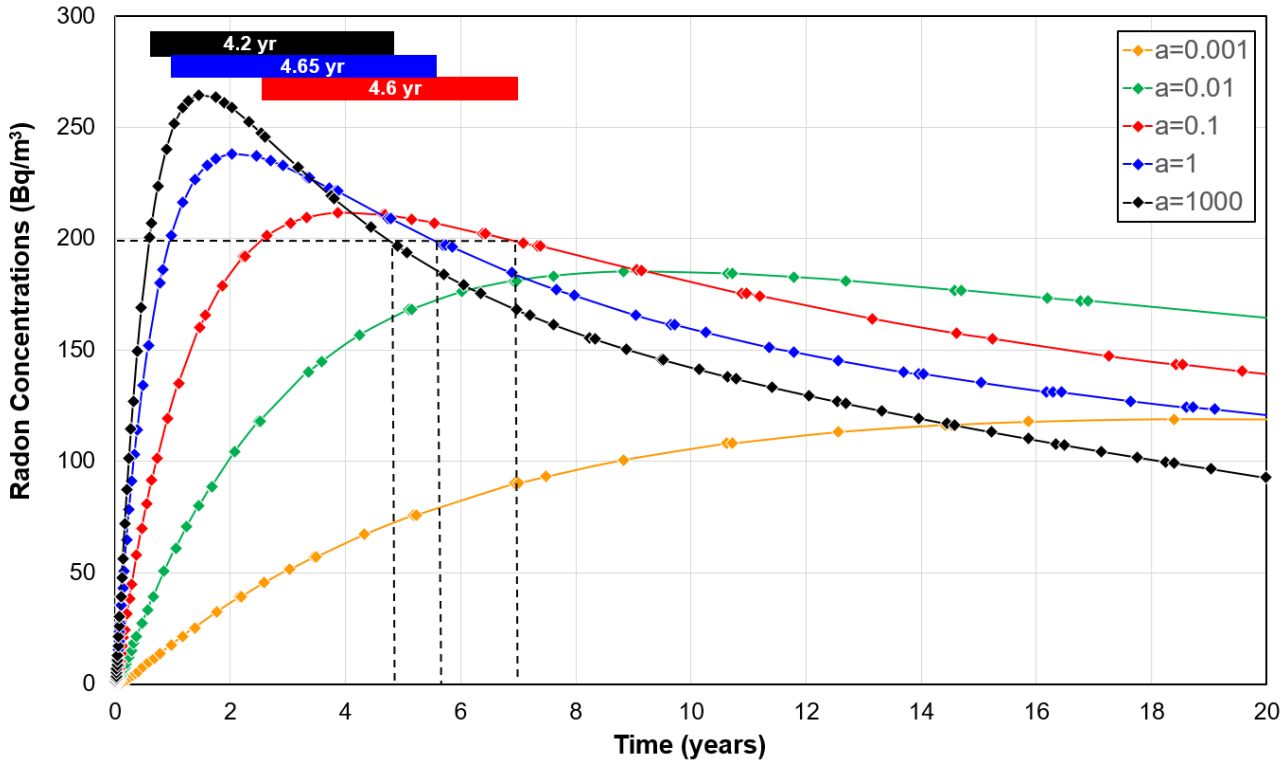

Figure 8. Evolution of the arithmetic mean radon concentration for quasi-instantaneous melt and four longer melt profiles approximating to 40% increase in diffusion coefficient after 0.5, 5, 50 and 500 years, as defined in the methodology, and *d*=2 m. Coloured bars show time above the 200 Bq/m^3 threshold.

In reality melting is likely to take place in step with seasonal temperature changes, which makes this modelling a very much simplified model. However, it does show that even if transport is solely diffusional, short time scale changes can lead to large changes in radon concentration in buildings.

3.5 Radon Transport Mechanisms

It is expected that radon transport will mainly occur by diffusion. However, there may be occasions where diffusion and advection occur concurrently. Initial modelling, indicates that added advection brings the peak in the radon concentration forward in time and increases its value significantly, but

also reduces the length of time values exceed the 200 Bq/m^3 threshold. The plume of radon passes more swiftly by being driven by advective flow, and might by-pass the building if the transport pathways around it are easier than through the building. There is also the possibility that radon dissolved in advectively driven water may add to the radon concentration in the building, however this transport mechanism was not modelled explicitly in this work.

It is also expected that the speed of permafrost melting will also have less effect for scenarios including significant advective transport. Once partially melting of permafrost leads to the development of connected pathways capable of sustaining flow they are expected to become dominant, reducing the sealing capacity of the remaining permafrost layer and resulting in short duration, barometrically-driven (Perrier and Girault, 2013), high intensity radon plumes which could be extremely dangerous. Further modelling will be required to confirm the implications of advective-diffusive radon transport.

It is clear that further modelling is needed and an exploration of diffusive and advectively-driven radon transport will be the subject of a future paper.

4 Discussion

The modelling presented in this paper represents only an initial study. The headline conclusion is that the melting of permafrost could expose a significant number of people to levels of radon in excess of the 200 Bq/m^3 threshold that many countries adopt.

We recognise five important qualifying issues to the main conclusion, some of which will reduce the impact of the results and some which amplify their importance.

First, all of the results discussed in this work are for unventilated buildings. Consequently, the results should all be considered to be worst-case scenarios.

Second, many of the northern community will be protected simply because their dwellings are well ventilated by traditional design, being built clear of the ground on piles (Buijze and Wright, 2021).

However, many of the more modern buildings are not constructed in this way, and one must also take account of modern commercial developments that are occupied by workers for the greater portion of the day.

Third, it is currently unclear how fast the permafrost melts. One might expect, and we show by modelling in this paper, that longer melt times mitigates against a sudden release of radon. However, not enough is known about the transport properties of permafrost to predict the development of its permeability as it degrades. It may not be true that a 40% partial melting of the permafrost results in a proportional increase in radon transport, as has been found for building materials with different water contents (Fournier et al., 2005). Rather, it is perfectly possible that a 5% partial melting of the permafrost might abruptly open fractures in the permafrost that would then act as radon superhighways.

Fourth, we have been forced to make a number of assumptions in the modelling, some of which can be removed in future modelling. One example of this is the imposition of seasonal variations in melting, perhaps based on field observations. The largest uncertainty in this modelling is the very sparse data concerning the storage, transport and partition of radon in water, gas, solid and ice phases within the permafrost and how these change as the permafrost melts. It is, consequently, a major recommendation of this work that experimental field and laboratory measurements are carried out to clarify this uncertainty.

Another assumption in the modelling is that there is no reduction of porosity upon thawing, which is to say that there is no compaction of the soil upon thawing. We know that such compaction does occur and is significant. Furthermore, such compaction amounts to a processes whereby radon can be 'pumped' out of the ground by the compaction process. Consequently, the results presented in this paper may represent less risk than is actually present.

Finally, it is well recognised that radon-acquired lung cancer is 25.8 (+5.4/-4.5) times more prevalent in tobacco smokers than it is for non-smokers (Darby et al., 2005). This is especially

important considering that the prevalence of smoking amongst the inhabitants of northern Canada and Greenland is approximately three times that of the global average of 21% (WHO, 2019). No data is available pertaining to the smoking rates in the northern Russian Federation, however, it is possible that smoking rates are significantly above the global mean here too. These populations would be very significantly sensitive to any release of radon which may occur as a result of permafrost melt.

5 Conclusions

We have used finite element modelling to examine the effect of permafrost melt due to climate change on radon exposure in buildings.

Initial modelling showed that a layer of permafrost provides an effective barrier to radon irrespective of whether the permafrost starts near the surface of starts at depths up to 15 m, with radon concentrations behind the barrier reaching up to 445.8 Bq/m^3 which is almost 12 times the value that would have been the case without the presence of the barrier. This represents a dynamic reservoir of radon if it were released.

It was confirmed that increases in the ability of gases to diffuse through permafrost caused by instantaneous partial melting resulted in the release of radon in a plume that raised the radon concentration in basement style buildings (either buried basements or basements resting on the surface) up to 350 Bq/m^3 and remaining greater than the 200 Bq/m^3 threshold for about 7 years for permafrost starting at the surface. Plumes were less intense and exceeded the threshold for shorter times as the depth to the top of the permafrost increased, until the peak radiation of the plumes were no longer exceeding the threshold.

Pile-constructed buildings exhibited no rise in radon at any time in the modelling.

Modelling was carried out to take account that melting of permafrost will not be instantaneous. Melting curves for the quasi-instantaneous case, and 40% melting occurring in 0.5, 5, 50 and 500 years were examined. For the first three of these cases the radon plume

provided domestic radon concentrations greather than the 200 Bq/m^3 threshold for between 4.2 and 4.65 years, but later values did not exceed the threshold, with the threshold limit occurring at about 15 years for a 40% melt.

Further modelling is being carried out to ascertain the effect of adding advective radon transport to the diffusion transport reported in this work, as well as to examine diurnal and seasonal melting of the permafrost.

We recognise that despite the problem of radon being allayed by good ventilation, the risk to the 5 million people live on permafrost in the Arctic Circumpolar Permafrost Region (ACPR) is high because (i) rocks underlying these regions provide more radon than the global average, (ii) radon has not previously been recognised as a problem in these areas due to the protective permafrost barrier, (iii) northern populations have smoking rates that are about 3 times the global mean and that radon-acquired lung cancer is 25.8 (+5.4/-4.5) times more prevalent in tobacco smokers than it is for non-smokers, and (iv) though traditional pile-constructed buildings still exist, more and more concrete basement-type buildings for homes, offices, shops and industry are being built.

Data availability

Data that support the discussion in this paper together with associated videos of the evolution of radon concentration with time are available at xxxxxxxx.

Acknowledgements

The author is grateful to M. Blouin for his help with initial modelling and also acknowledges development funding from The University of Leeds.

References

Ahn, J., Headly, M., Wahlen, M., Brook, E.J., Mayewski, P.A. and Taylor, K.C. (2008). CO_2 diffusion in polar ice: Observations from naturally formed CO_2 spikes in the Siple Dome (Antarctica) ice core. *Journal of Glaciology* **54(187)**, 685-695.

Al-Zoughool, M. & Krewski, D. (2009). Health effects of radon: A review of the literature, *International Journal of Radiation Biology* 85(1), 57-69.

Barrio-Parra, F., Hidalgo, A., Izquierdo-Díaz, M., Arévalo-Lomas, L. and De Miguel, E. (2022). 1D_RnDPM: A freely available 222Rn production, diffusion, and partition model to evaluate confounding factors in the radon-deficit technique. *Science of the Total Environment* **807.**

BEIR VI. *Biological Effects of Ionizing Radiation VI Report. Health effects of exposure to indoor radon*. (National Academy Press, Washington DC, 1999).

Bjerregaard, P., Mulvad, G. & Pedersen, H.S. (1997). Cardiovascular risk factors in Inuit of Greenland, *Int. J. Epidemiology* **26(6)**, 1182-1190.

Buijze, J.A.J.C. & Wright, A.J. (2021). The potential for the Passive House standard in Longyearbyen – the High Arctic. *Building Services Engineering Research and Technology* **42(3)**, 307-325.

Chen, C., Thomas, D.M. & Green, R.E. (1995). Modeling of radon transport in unsaturated soil. *J. Geophys. Res.* **100(B8)**, 15,517-15,525.

Chung, L.K., Mata, L.A., Carmona, M.A., Shubayr, N.A.M., Zhou, Q., Ye, Y. & Kearfott, K.J. (2020). Radon kinetics in a natural indoor radon chamber. *Science of the Total Environment* **734**, 139167.

Chuvilin, E., Grebenkin, S. & Zhmaev, M. (2021). Gas permeability of sandy sediments: Effects of phase changes in pore ice and gas hydrates. *Energy and Fuels* **35(9)**, 7874-7882.

Conen, F. and Robertson, L.B. (2002). Latitudinal distribution of radon-222 flux from continents. *Tellus, Series B: Chemical and Physical Meteorology*, **54(2)**, 127-133.

Cozmuta, I., van der Graaf, E.R. & de Meijer, R.J. (2003). Moisture dependence of radon transport in Concrete: Measurements and modeling. *Health Phys.* **85(4)**, 438–456.

Darby, S., Hill, D., Auvinen, A., Barros-Dios, J.M., Baysson, H., Bochicchio, F., Deo, H., Falk, R., Forastiere, F., Hakama, M., Heid, I., Kreienbrock, L., Kreuzer, M., Lagarde, F., Mäkeläinen, I., Muirhead, C., Oberaigner, W., Pershagen, G., Ruano-Ravina, A., Ruosteenoja, E., Schaffrath Rosario, A., Tirmarche, M., Tomášek, L., Whitley, E., Wichmann, H.E. & Doll, R. (2005). Radon in homes and risk of lung cancer: collaborative analysis of individual data from 13 European case-control studies. *BMJ* **330(7485)**, 223-227.

Darby, S., Hill, D., Deo, H., Auvinen, A., Barros-Dios, J.M., Baysson, H., Bochicchio, F., Falk, R., Farchi, S., Figueiras, A., Hakama, M., Heid, I., Hunter, N., Kreienbrock, L., Kreuzer, M., Lagarde, F., Mäkeläinen, I., Muirhead, C., Oberaigner, W., Pershagen, G., Ruosteenoja, E., Rosario, A.S., Tirmarche, M., Tomášek, L., Whitley, E., Wichmann, H. & Doll, R. (2006). Residential radon and lung cancer - Detailed results of a collaborative analysis of individual data on 7148 persons with lung cancer and 14208 persons without lung cancer from 13 epidemiologic studies in Europe. *Scandinavian Journal of Work, Environment and Health Supplement* **32(1)**, 1-84.

Dela Cruz, C.S., Tanoue, L.T. & Matthay, R.A. (2011). Lung Cancer: Epidemiology, Etiology, and Prevention. *Clin Chest Med*. **32(4)**, 605-644.

Eichler, B., Zimmermann, H.P., and Gäggeler, H.W. (2000). Adsorption of radon on ice surfaces, *J. Phys. Chem. A* **104**, 3126-3131.

Fortin, G., Van Bochove, E., Jones, H.G., Thériault, G. & Bernier, M. (2007). The simultaneous determination of air permeability and gas diffusion through ice layers in the field. *Nordic Hydrology* **38(3)**, 203-210.

Fournier, F., Groetz, J., Jacob, M., Crolet, J.M. & Lettner, J.M. (2005). Simulation of radon transport through building materials: Influence of the water content on radon exhalation rate. *Transport in Porous Media*, **59(2)**, 197-214.

Gadd, M.S. and Borak, T.B. (1995). In-situ determination of the diffusion coefficient ^{222}Rn in concrete, *Health Phys*. **68(6)**, 817–822.

Ikeda-Fukazawa, T., Kawamura, K. and Hondoh, T. (2004a). Diffusion of nitrogen gas in ice Ih. *Chemical Physics Letters* **385(5-6)**, 467-471.

Ikeda-Fukazawa, T., Kawamura, K. and Hondoh, T. (2004b). Mechanism of molecular diffusion in ice crystals. *Molecular Simulation* **30(13-15)**, 973-979.

Krewski, D., Lubin, J.H., Zielinski, J.M., Alavanja, M., Catalan, V.S., Field, R.W., Klotz, J.B., Létourneau, E.G., Lynch, C.F., Lyon, J.I., Sandler, D.P., Schoenberg, J.B., Steck, D.J., Stolwijk, J.A., Weinberg, C. & Wilcox, H.B. (2005). Residential radon and risk of lung cancer: A combined analysis of 7 North American case-control studies. *Epidemiology* **16(2)**, 137-145.

Krewski, D., Lubin, J.H., Zielinski, J.M., Alavanja, M., Catalan, V.S., Field, R.W., Klotz, J.B., Létourneau, E.G., Lynch, C.F., Lyon, J.L., Sandler, D.P., Schoenberg, J.B., Steck, D.J., Stolwijk, J.A., Weinberg, C. & Wilcox, H.B. (2006). A combined analysis of north American case-control studies of residential radon and lung cancer. *Journal of Toxicology and Environmental Health - Part A* **69(7-8)**, 533-597.

Lubin, J.H., Wang, Z.Y., Boice JR., J.D., Xu, Z.Y., Blot, W.J., De Wang, L. & Kleinerman, R.A. (2004). Risk of lung cancer and residential radon in China: Pooled results of two studies. *Int. J. Cancer* **109(1)**, 132-137.

Moldrup, P., Olesen, T., Schjonning, P., Yamaguchi, T., Rolston, D.E. (2000). Predicting the Gas Diffusion Coefficient in Undisturbed Soil from Soil Water Characteristics, *Soil Sci Soc Am J* **64**, 94-100.

Nazaroff, W. (1992). Radon transport from soil to air. *Rev. Geophys*. **30**, 137–160.

Nitzbon, J., Westermann, S., Langer, M., Martin, L.C.P., Strauss, J., Laboor, S. & Boike, J. (2020). Fast response of cold ice-rich permafrost in northeast Siberia to a warming climate. *Nature Communications* **11(1)**, 2201.

Ongori, J.N., Lindsay, R. and Mvelase, M.J. (2015). Radon transfer velocity at the water-air interface. *Applied Radiation and Isotopes* **105**, 144-149.

Othman, N.D., Rashid, A.S.A., Hashim, S., Sanusi, M.S.M. & Bery, A. (2021). Radon gas migration through soil – A review. *Journal of Mines, Metals and Fuels*, **69(8)**, 3-8.

Pawel, D.J. & Puskin, J.S. (2003). EPA assessment of risks from radon in homes, *United States Environmental Protection Agency Report* EPA 402-R-03-003.

Peng, X., Zhang, T., Frauenfeld, O.W., Du, R., Jin, H. and Mu, C. (2021). A Holistic Assessment of 1979–2016 Global Cryospheric Extent. *Earth's Future*, 9(8).

Perrier, F. and Girault, F. (2013). Harmonic response of soil radon-222 flux and concentration induced by barometric oscillations. Geophysical Journal International, 195(2), pp. 945-971.

Peto, J. and Darby, S. (1994). Radon risk reassessed. *Nature* **368(6467)**, 97-98.

Petrov, O. & Pubellier, M. *Tectonic map of the arctic*. Commission for the geologic map of the world (CGMW-VSEGEI, ISBN: 978-29173-10366, 2018)

Ramage, J., Jungsberg, L., Wang, S., Westermann, S., Lantuit, H. & Heleniak, T. (2021). Population living on permafrost in the Arctic. *Population and Environment*, **43(1)**, 22-38.

Rogers, V.C. and Nielson, K.K. (1991a). Multiphase radon generation and transport in porous material, *Health Phys.* **60(6),** 807–815.

Rogers, V.C. and Nielson, K.K. (1991b). Correlations for predicting air permeabilities and ^{222}Rn diffusion coefficients of soils, *Health Phys*. **61(2),** 225–230.

Scheib, C., Appleton, J.D., Miles, J.C.H., Green, B.M.R., Barlow, T.S. & Jones, D.G. (2009). Geological controls on radon potential in Scotland. *Scottish Journal of Geology* **45(2)**, 147-160.

Turetsky, M.R., Abbott, B.W., Jones, M.C., Anthony, K.W., Olefeldt, D., Schuur, E.A.G., Grosse, G., Kuhry, P., Hugelius, G., Koven, C., Lawrence, D.M., Gibson, C., Sannel, A.B.K. & Mcguire, A.D. (2020). Carbon release through abrupt permafrost thaw. *Nature Geoscience* **13(2)**, 138-143.

UNSCEAR. (2000). United Nations Scientific Committee on the Effects of Atomic Radiation. *Sources and Effects of Ionizing Radiation. UNSCEAR 2000 Report to the General Assembly, with Scientific Annexes.*

WHO. *WHO Handbook on Indoor Radon, A Public Health Perspective, ed.* Zeeb, H. & Shannoun, F. (World Health Organisation, Geneva, 2009).

WHO. *WHO global report on trends in prevalence of tobacco use 2000–2025*, third edition (World Health Organization, Geneva, 2019).

Worsley, P. (1986). Palaeoclimate: Permafrost and ice-wedge growth, *Nature* **322**, 683-684.

Witze, A. (2020). The Arctic is burning like never before - and that's bad news for climate change. *Nature* **585(7825)**, 336-337.

Yumashev, D., Hope, C., Schaefer, K., Riemann-Campe, K., Iglesias-Suarez, F., Jafarov, E., Burke, E.J., Young, P.J., Elshorbany, Y. & Whiteman, G. (2019). Climate policy implications of nonlinear decline of Arctic land permafrost and other cryosphere elements. *Nature Communications*, **10(1)**, 1900.